MULTIPLE FREQUENCY RANGE IMAGING TO REMOVE MEASUREMENT AMBIGUITY

Andrew D. Payne[1], Adrian P. P. Jongenelen[2], Adrian A. Dorrington[1], Michael J. Cree[1], Dale A. Carnegie[2]
[1]Dept. Engineering, The University of Waikato, Private Bag 3105, Hamilton, New Zealand.
[2]School of Chemical and Physical Sciences, Victoria University of Wellington, PO Box 600, Wellington, New Zealand.
Email: a.payne@waikato.ac.nz

Abstract: Range imaging systems use a specialised sensor to capture an image where object distance (range) is measured for every pixel using time-of-flight. The scene is illuminated with an amplitude modulated light source, and the phase of the modulation envelope of the reflected light is measured to determine flight time, hence object distance for each pixel. As the modulation waveform is cyclic, an ambiguity problem exists if the phase shift exceeds 2π radians. To overcome this problem we demonstrate a method that superposes two different modulation frequencies within a single capture. This technique reduces the associated overhead compared with performing two sequential measurements, allowing the system to retain high range measurement precision at rapid acquisition rates. A method is also provided to avoid interference from aliased harmonics during sampling, which otherwise contaminate the resulting range measurement. Experimental results show the potential of the multiple frequency approach; producing high measurement precision while avoiding ambiguity. The results also demonstrate the limitation of this technique, where large errors can be introduced through a combination of a low signal to noise ratio and suboptimal selection of system parameters.

1. INTRODUCTION

Range imaging is an emerging technology capable of measuring the size, shape and locations of objects by measuring intensity and distance (range) for every pixel in an image. Unlike laser scanners, range imaging systems measure every pixel simultaneously without the need for moving parts; leading to a potentially cheap, fast and compact measurement device suitable for a wide range of applications including machine vision, gesture recognition for gaming systems, and automotive and security applications.

Distance is determined from an indirect time-of-flight measurement, where the entire scene is illuminated with an amplitude modulated light source and the light is reflected from objects back to a specialised image sensor, as illustrated in Figure 1. The time required for the light to travel to and from each object (the flight time) results in a phase shift of the illumination modulation envelope proportional to the distance travelled. The phase shift is then measured independently by each pixel to determine the object distance. This is achieved by modulating the sensor pixel gain at the same frequency as the light source (homodyne

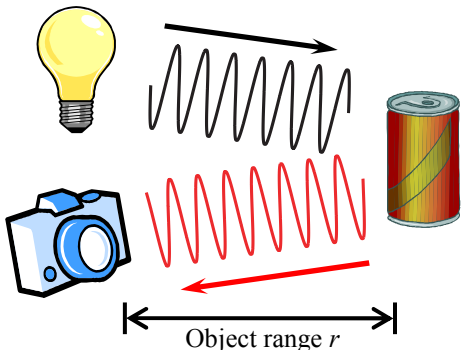

Figure 1: Object distance is determined by measuring the modulation envelope phase of the reflected light within each pixel in the image sensor.

operation), and integrating the signal, effectively performing a correlation between the illumination and sensor waveforms. The data is readout from the sensor, and sensor modulation is phase stepped by $\theta=\frac{\pi}{2}$ (90°) before capturing the next sample i. From N=4 samples, $I_0,\ldots I_3$, the phase shift φ, amplitude A, and background (or ambient) offset B of the received light can be calculated using (1)–(3).

$$\varphi = \tan^{-1}\left(\frac{\Sigma\left(I_i \cos\theta_i\right)}{\Sigma\left(I_i \sin\theta_i\right)}\right) = \tan^{-1}\left(\frac{I_0 - I_2}{I_1 - I_3}\right) \tag{1}$$

$$A = \frac{\sqrt{\left[\Sigma\left(I_i \cos\theta_i\right)\right]^2 + \left[\Sigma\left(I_i \sin\theta_i\right)\right]^2}}{2} = \frac{\sqrt{\left(I_0 - I_2\right)^2 + \left(I_1 - I_3\right)^2}}{2} \tag{2}$$

$$B = \frac{\Sigma I_i}{N} = \frac{I_0 + I_1 + I_2 + I_3}{4} \tag{3}$$

Object range r is then computed from the phase measurement φ using (4), where f is the modulation frequency of the illumination source and image sensor, and c is the speed of light.

$$r = \frac{\varphi}{2\pi} \cdot \frac{c}{2f} \tag{4}$$

2. RANGE AMBIGUITY

Phase is cyclic; if the phase shift of the illumination signal exceeds 2π radians, it will be wrapped around to fall within the range of 0 to 2π during the calculation in (1). This means that objects which are located at distances greater than

$$R = \frac{c}{2f}, \tag{5}$$

known as the unambiguous range, will be incorrectly calculated using (4). For example, for a modulation frequency of 30 MHz where the unambiguous range is 5 m, objects located at 1.25 m and 6.25 m both have a phase value φ of π/2; therefore both objects will result in a computed range of 1.25 m. To correct this error, (4) can be modified as (6), where an integer multiple of the unambiguous distance is added by the integer variable x. In this example x equals one for the distant object, resulting in the correct 6.25 m computed range value. The

difficulty is that x cannot be resolved directly from the four captured samples above, limiting the working distance of the system to the unambiguous range.

$$r = \left(\frac{\varphi}{2\pi} + x \right) \frac{c}{2f} \tag{6}$$

2.1. Reduction of the modulation frequency

The simplest method to avoid ambiguity problems is to reduce the modulation frequency f, to increase the unambiguous range. For example, a modulation frequency f of 30 MHz corresponds to a 5 m unambiguous range, whereas a modulation frequency of 10 MHz will provide 15 m. An appropriate frequency can therefore be selected to encompass all object ranges within a given scene, and ambiguity can be avoided.

However, range measurement uncertainty is also dictated by the selection of modulation frequency, as the standard deviation σ is given by [1]

$$\sigma = \frac{c}{4\sqrt{2}\pi f} \cdot \frac{\sqrt{B + A}}{c_d A}, \tag{7}$$

where the additional term c_d is called the demodulation contrast. A reduction of the modulation frequency proportionally increases measurement uncertainty, and is therefore not suitable for applications which require high precision.

2.2. Pseudo-noise modulation

Instead of continuous sinusoidal amplitude modulation of the illumination source, it is possible to use a digitally generated pseudo-random sequence. The main advantage of this technique is that multiple range imaging cameras can operate within the same scene, with minimal interference between the different illumination sources [1]. A secondary effect is that objects beyond the working distance fall outside the correlation peak and the distance cannot be measured [1]. Although this technique does not allow extended distances to be measured, the benefit of this approach is that objects which occur beyond the system working distance can be identified and removed from the data.

2.3. Consecutive measurements at different frequencies

Another demonstrated method of resolving measurement ambiguity is to perform two sequential measurements at different modulation frequencies [2]. In this instance two high modulation frequencies are used, f_a and f_b, each producing a different unambiguous range. By comparing the two possible sets of range values (r_a at f_a and r_b at f_b) using (6) with x=1,2,3…, only one distance will be common to both measurements. An example is shown in Figure 2 where an object captured using 40 MHz and 33.3 MHz modulation frequencies has phase shift φ equal to $\frac{4}{3}\pi$ and $\frac{4}{9}\pi$ respectively. Only one common location exists between the two captures (at 10.00 m); hence this is selected as the true range and ambiguity from each of the measurements is resolved. This simple method allows the unambiguous range to be extended to

$$R = \frac{c}{2 \cdot |f_a - f_b|}, \tag{8}$$

significantly extending the working range of the system. An advantage of this technique is that the two measurements can be averaged together to produce a root two improvement in measurement precision. However, this comes at the expense of doubling the total number of samples of the illumination waveform, thereby doubling the acquisition time. To maintain a rapid acquisition time the sample integration time can be reduced; however this at the expense of measurement precision as discussed further in section 2.4.

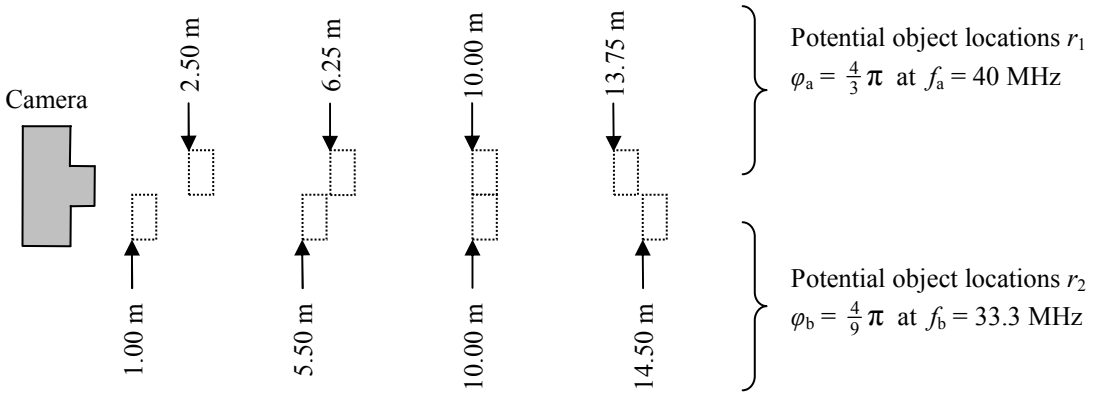

Figure 2: A single object produces multiple ambiguous range values for a single modulation frequency. By comparing two different modulation frequencies, the true object location (10.00 m) can be resolved.

2.4. Simultaneous measurement of multiple frequencies

Performing two consecutive measurements, as in section 2.3, essentially involves collecting eight samples of the waveform(s) to determine only five variables; the background illumination B, and the phase φ_a, φ_b and amplitude A_a, A_b of the two modulation frequencies respectively. Part of the problem is that the background illumination B is actually measured twice – once at each modulation frequency. It is therefore apparent that performing two consecutive measurements is not an efficient method to resolve ambiguity.

An alternate approach is to superpose the two modulation frequencies so that they can be measured simultaneously. To allow the two amplitudes and phases to be independently measured, a different phase step size θ must be selected for each of the two modulation frequencies. An example is to use $\theta_a = \frac{2\pi}{5}$ (72°) for the first modulation frequency and $\theta_b = \frac{4\pi}{5}$ (144°) for the second modulation frequency, while capturing a total of N=5 sample images. Using this approach the first modulation frequency is sampled five times over a 2π radian phase shift, while the second modulation frequency is sampled five times over a 4π shift, effectively being sampled at half the sampling rate. A Discrete Fourier Transform (DFT) of the five samples can then be used to calculate the DC component, and amplitude and phase of the two modulation frequencies which now fall in different frequency bins. In this situation, the selection of N=5 is most efficient because the minimum number of samples are acquired to determine the five unknown variables.

The major advantage of this technique is that the total number of captured image frames can be reduced compared with the use of consecutive measurements in section 2.3. At the end of the integration period for each image frame, the data must read out of the sensor before acquisition of the next image can begin. During this read out time the sensor does not collect any incoming light. By using only five, rather than eight, image frames, the total readout time is reduced and the integration period for each sample can be extended to capture more light to

increase the signal amplitude A, and therefore improve measurement precision according to (7). This is particularly significant for high speed operation where range images are required at video frame rates and the integration time is relatively short. For example, assuming an application requires an update rate of 25 range images per second and the sensor takes 2.5 ms to read out each image; to capture eight raw images there is 2.5 ms available to integrate each image (the same length of time as the read out). In this configuration the sensor is only sensitive to the incoming light 50% of the time. To provide the same 25 range images per second processed from five captured images, the integration time can be increased to 5.5 ms, and the sensor will be sensitive to the incoming light for over twice as long for each raw image.

To create the superposed modulation waveform, two sinusoidal waveforms at frequency f_a and f_b can simply be added together as shown on the left hand side of Figure 3. The illumination source and image sensor are then amplitude modulated with this waveform. In practice however, range imaging systems often approximate the sinusoidal waveform by using square wave modulation [3, 4], generated using a digital source to simplify the electronic design. The superposed waveform cannot be approximated in the same manner using a digital source; therefore an alternate method of combining the two waveforms is shown on the right hand side of Figure 3. By dividing the sensor integration time in half, the two modulation frequencies can be applied sequentially *within a single image frame*, using the integrating function of the image sensor to sum the result. The sensor output is identical to a true superposed waveform, with the advantage that the technique is compatible with the existing practise of using digital switching to approximate each of the sinusoidal waveforms.

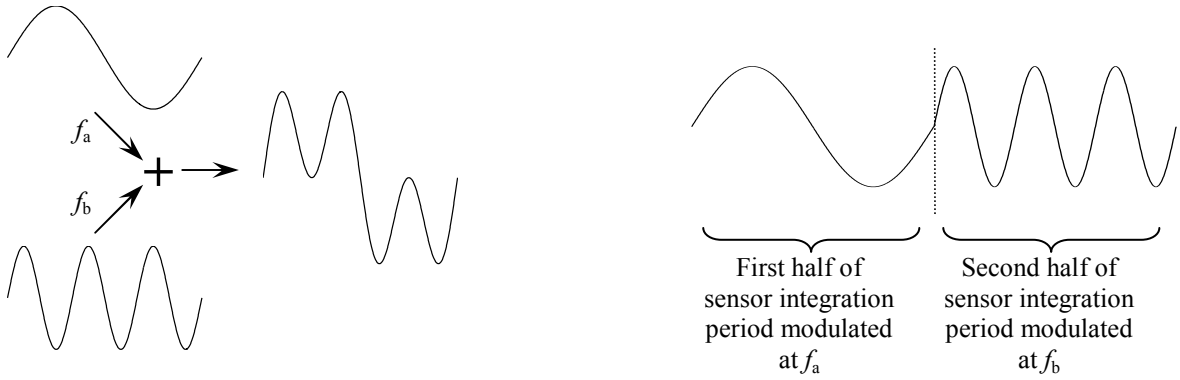

Figure 3: Left: Two sinusoidal waveforms at frequencies f_a and f_b are superposed to create the sensor and light source modulation waveform. Right: The same effect can be created by dividing the sensor integration period in two, and switching between f_a and f_b for each captured image.

2.5. Nonlinearity due to harmonics

The use of a digital square wave to approximate the sinusoidal amplitude modulation introduces a systematic error in the resulting range measurement. This error is due to the higher order harmonics present in the square wave being aliased onto the signal of interest during the sampling process [5–7]. Typically a correction is generated through calibration [6], which can then be applied during post processing. When two modulation frequencies are superposed as described in section 2.4, the calibration routine becomes significantly more complex as each signal has the potential to interfere not only with itself (as in the typical

single frequency case), but also with the other frequency. Candidate harmonics which are aliased onto each of the two signals of interest are given by

$$n_{a\to a} = i\frac{2\pi}{\theta_a} \pm 1, \qquad n_{b\to a} = i\frac{2\pi}{\theta_b} \pm \frac{\theta_a}{\theta_b}, \qquad n_{b\to b} = i\frac{2\pi}{\theta_b} \pm 1, \qquad n_{a\to b} = i\frac{2\pi}{\theta_a} \pm \frac{\theta_b}{\theta_a}, \tag{9}$$

adapted from [8], where i=0,1,2,3… and n is the harmonic number which is valid only for integer values. The subscript notation indicates the source of the harmonic and the signal it will be aliased onto, e.g. $n_{a\to a}$ refers to harmonics from modulation frequency f_a being aliased onto f_a (i.e. itself), while $n_{a\to b}$ refers to harmonics from modulation frequency f_a falling on modulation frequency f_b during sampling.

The most efficient sampling approach described in section 2.4 uses N=5 with $\theta_a=\frac{2\pi}{5}$ and $\theta_b=\frac{4\pi}{5}$. Substituting these values into the four equations in (9), there are a significant number of candidate harmonics which could potentially interfere with each of the two measurements. By increasing the number of samples, i.e. N=6 with $\theta_a=\frac{\pi}{3}$ and $\theta_b=\frac{2\pi}{3}$, $n_{b\to a}$ does not contain any integer values (i.e. no harmonics from modulation frequency f_b are aliased onto frequency f_a) while $n_{a\to a}$ contains only odd harmonics (5,7,11,13,17,19…). A prior technique has been demonstrated where it is possible to reject odd harmonics during the sampling process [7], removing the $n_{a\to a}$ aliased harmonics. It is therefore possible to perform a range measurement at modulation frequency f_a without any distortion due to harmonics, avoiding the need to perform calibration/compensation on the measurement data to remove this source of error.

With N=6, the second modulation frequency f_b still suffers from aliasing even if odd harmonics are rejected ($n_{b\to b}$=2,4,5,7,8,10… and $n_{a\to b}$=2,4,8,10,14,16…), so rather than trying to perform a high precision measurement at the second modulation frequency as in [2], it is proposed that a low modulation frequency can instead be substituted as described in section 2.1. The result from this low frequency measurement will produce an unambiguous approximation of the object range for each pixel, which can be used to remove ambiguity from the high frequency, high precision measurement.

3. Experimental results

An image intensifier based range imaging system was utilised to study the practicality of the dual–modulation frequency approach described above. The system is shown in Figure 4, and further detail can be found in [2]. The advantage of this particular system is that the modulation frequency can be set much higher than other range imaging devices (up to 100 MHz) to achieve high range measurement precision; but ambiguity problems also escalate at these frequencies as the unambiguous range R reduces as given by (5).

A scene was constructed from cardboard boxes placed at different distances as shown in Figure 4, and the range imaging system was configured with f_a=83.3 MHz, $\theta_a=\frac{\pi}{3}$ and f_b=12.8 MHz, $\theta_b=\frac{2\pi}{3}$. The lower modulation frequency f_b provides an unambiguous range R of 11.7 m, compared to only 1.8 m if f_a had been used alone in a traditional single frequency configuration. The camera frame rate was set to 90 fps, allowing 15 range images to be captured per second (using six frames per capture) with a resolution of 256×256 pixels. The object distances were measured as 1.708, 2.796, 3.512, 3.506, 4.599, 5.318, 5.310, and 5.707 m respectively using a Leica Distro Plus laser distance meter. An example of the captured data is given in the top of Figure 5 for two single pixels located at objects 2 and 4 respectively, with a reconstruction of the received modulation waveform showing how the

waveform shape is significantly different to the traditional sinusoid. Equations (1)–(3), which are equivalent to performing a Discrete Fourier Transform (DFT), are used to extract the background illumination B, and amplitude A and phase φ for each of the modulation frequencies which are located in different frequency bins as illustrated in Figure 5.

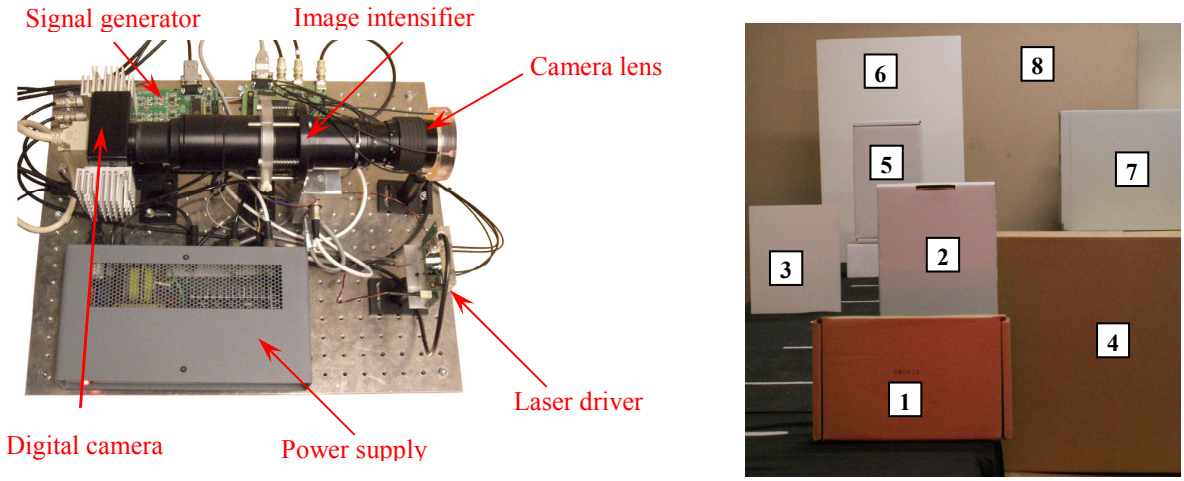

Figure 4: Left: Photo of the image intensifier based range imaging system; Right: A photo of objects at various distances within the scene.

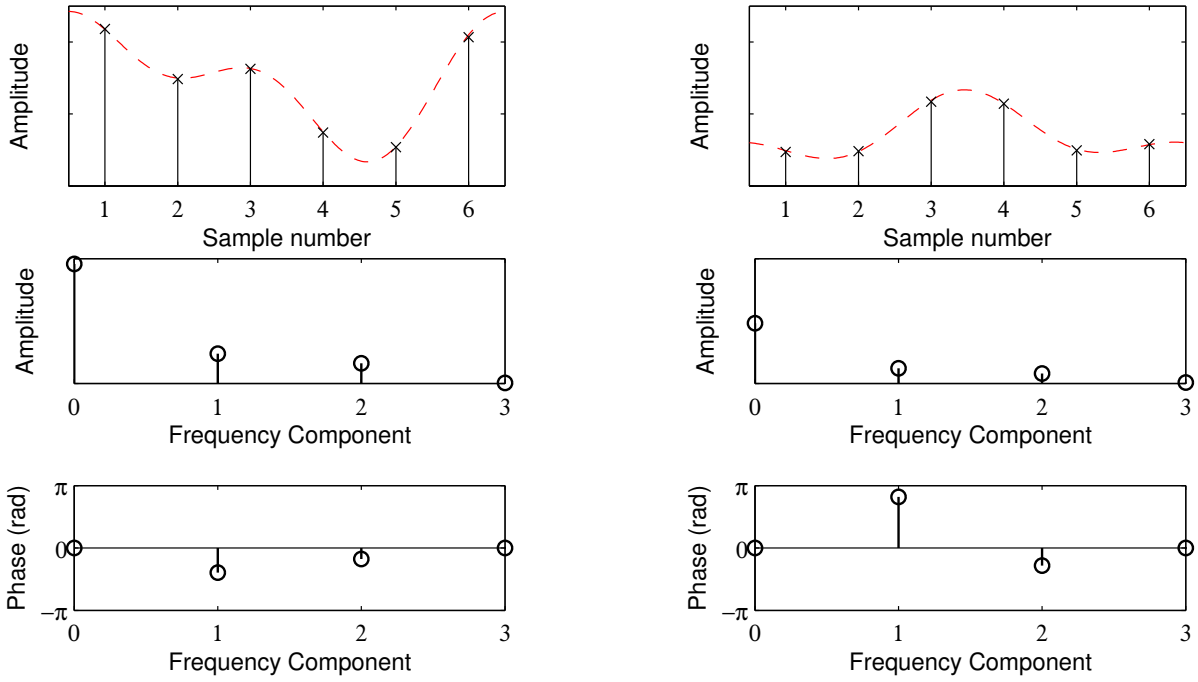

Figure 5: Top: Raw captured data for a single pixel located at object 2 (left) and object 4 (right). The dashed line illustrates the reconstructed received illumination waveform. Centre and bottom: Amplitude and phase calculated using a DFT on the six samples.

Range values were independently calculated using (4) for the two measured phase values at the two different modulation frequencies, and the results are shown in the left and centre of Figure 6. At the high modulation frequency f_a=83.3 MHz, objects 1,3,4,6,7 all appear to be located at the same distance of approximately 1.2 m, and objects 2 and 5 appear at a distance

of approximately 0.5 m due to ambiguity in the range measurement. The low frequency f_b=12.8 MHz range image in the centre of Figure 6 does not suffer from the ambiguity problem, but the measurement noise is relatively high.

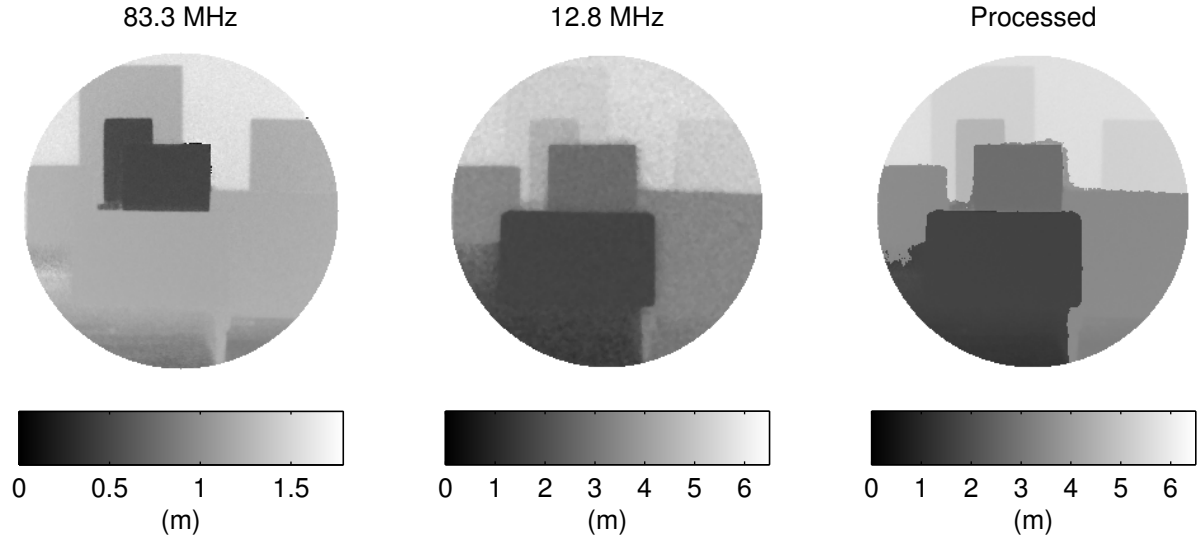

Figure 6: Left: Ambiguous range data captured using a high modulation frequency where objects at different distances are indistinguishable; Centre: Unambiguous range data captured with a low modulation frequency, with a corresponding high noise level; Right: Processed range image from the two data sets, providing unambiguous range with high precision.

The processed scene is shown on the right hand side of Figure 6, where data from the two range images have been combined. The resultant range image is comprised of the precise data from the high frequency measurement f_a, where contamination due to harmonics has been avoided as described in section 2.5, combined with the low frequency f_b data, which is used to calculate the most probable value of x in (6) and thereby remove ambiguity.

3.1. Measurement precision

To determine the measurement precision of the range images, the scene was captured fifty times and the variation at each pixel was calculated from the (one–sigma) standard deviation of the measured range. A region of 15×15 pixels was then selected from each object to give a representation of the performance for different distances and object properties, with the result shown by the triangle marker in Figure 6. The precision varied from approximately 1.2 cm for a close object, to 4.7 cm at the far wall. For comparison purposes, a traditional single frequency measurement was also performed using f=12.8 MHz, with four samples (N=4) shifted by $\theta=\frac{\pi}{2}$ (90°). As only four samples are captured in this instance (as opposed to six for the multiple frequency technique), the integration time for each raw image frame was extended while still maintaining an identical 15 range images per second. The resulting standard deviation varied between approximately 2.9 cm to 8.9 cm as shown by the cross marker in Figure 6, where on average the uncertainty was about double that of the multiple frequency approach.

A further improvement in precision can be found by realising that the low frequency measurement f_b intentionally only contributes the initial approximation of the object location, as the data is noisy due to the low modulation frequency and is likely to be experience small

systematic errors due to harmonics. As this data does not contribute towards measurement precision, the division of the integration time can be changed to favour the high frequency measurement f_a. By increasing the percentage of time at the high frequency, the proportional increase in signal amplitude A_a will reduce the measurement error. An example is given in Figure 6 where 75% of the integration time was at f_a=83.3 MHz, with only 25% of the time at f_b=12.8 MHz. The measurement uncertainty is expected to be reduced by approximately 20% in this case as given by (7), but the data in Figure 6 shows the uncertainty reducing by about 40%, with values from 0.7 to 2.6 cm. This difference might be explained by the contribution of other noise sources within the system that are not accounted for in the theoretical precision limit given by (7).

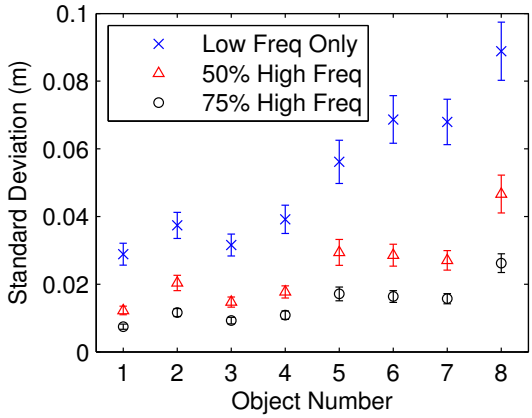

Figure 6: Measurement precision at each object over 50 consecutive captures. The triangle marker shows precision for the multiple frequency technique where the integration time is split equally (50%) between f_a and f_b. To improve measurement precision, a larger percentage (75%) of the integration time was given to the high frequency measurement f_a, as illustrated by the circle marker. Finally, a standard single frequency capture is provided by the cross marker for comparison.

By further altering the integration time ratio between f_a and f_b, it would be expected that continued improvement of the measurement uncertainty would ensue; however noise within the low frequency measurement precludes the use of this approach. Additional data (not shown here) was collected with up to 95% of the integration time at the high modulation frequency f_a. At these ratios, noise in the low frequency measurement meant that the integer x in (6) could not be correctly determined, and the range values at some pixels were incorrect by some metres (an integer multiple of the unambiguous range value R). A similar effect can already be seen on the edges of some of the objects in the processed data in Figure 6, particularly between the transition of objects 2 and 8 (the rear wall), where shadowing, focusing issues and other limitations have resulted in a few pixels appearing at an incorrect distance. In this case, post processing could be used to identify regions that are likely to be problematic, e.g. where the signal amplitude is low, and these points could be removed.

4. Evaluation and conclusion

The experimental results have verified that the amplitude and phase can be successfully extracted from two different modulation frequencies superposed within a single capture, providing an efficient method to remove ambiguity from the resultant range measurement. Systematic errors from aliased harmonics are also avoided through selection of the phase step

size, and the use of harmonic rejection during the sampling process, removing the need for calibration or the need to apply compensation to the resultant measurement data.

The experimental data demonstrates that the overall measurement performance is dependent on the division of the integration time between the high modulation frequency f_a, which contributes the measurement precision, and the low modulation frequency f_b, which allows ambiguity to be removed. The optimal ratio of the two modulation frequencies for a given scene will therefore maximise the high frequency integration time without significantly deteriorating the low frequency measurement accuracy. This, however, is the main limitation of the proposed system. The processed range data does not degrade gracefully as noise increases, instead producing measurements which can be metres from the true location. As the measurement signal to noise ratio is scene dependent, the optimal integration ratio will also be scene dependent; therefore it is not possible to select one optimal ratio for all situations.

Although it is likely possible to detect and remove rogue range measurements during post processing, e.g. by simply applying a median filter to the data, future work will instead focus on the superposition of two high frequency modulation waveforms, where object range is calculated as described in section 2.3. The advantage to this approach is that 100% of the integration time contributes towards measurement precision, resulting in improved overall performance compared to that presented here. In this instance further investigation of the harmonic content of the modulation waveforms and cancellation techniques is required to avoid the need to characterise and compensate for resulting systematic errors due to aliasing.

References:

[1] B. Büttgen and P. Seitz, "Robust Optical Time-of-Flight Range Imaging Based on Smart Pixel Structures," IEEE Transactions on Circuits and Systems I: Regular Papers, vol. 55, pp. 1512-1525, 2008.

[2] A. A. Dorrington, M. J. Cree, A. D. Payne, R. M. Conroy, and D. A. Carnegie, "Achieving sub-millimetre precision with a solid-state full-field heterodyning range imaging camera," Meas. Sci. Technol., vol. 18, pp. 2809-2816, 2007.

[3] R. Schwarte, "Breakthrough in multichannel laser-radar technology providing thousands of high-sensitive lidar receivers on a chip," Proceedings of SPIE, vol. 5575, pp. 126-136, 2004.

[4] S. Hsu, S. Acharya, A. Rafii, and R. New, "Performance of a Time-of-Flight Range Camera for Intelligent Vehicle Safety Applications," Advanced Microsystems for Automotive Applications 2006, pp. 205-214, 2006.

[5] R. Lange, "3D Time-of-Flight Distance Measurement with Custom Solid-State Image Sensors in CMOS/CCD-Technology," Ph.D. dissertation, University of Siegen, 2000.

[6] T. Kahlmann and H. Ingensand, "High-precision investigations of the fast range imaging camera SwissRanger (TM)," Proc. SPIE Photonics in the Transportation Industry: Auto to Aerospace, vol. 6758, pp. 67580J, 2007.

[7] A. D. Payne, A. A. Dorrington, M. J. Cree, and D. A. Carnegie, "Improved Linearity Using Harmonic Error Rejection in a Full-Field Range Imaging System," Proc. SPIE 3D Image Capture and Applications VII, vol. 6805, pp. 68050D, 2008.

[8] A. A. Dorrington, A. D. Payne, and M. J. Cree, "Harmonic contamination in multiple frequency modulation range imaging systems," SPIE Journal of Electronic Imaging Letters, in preparation.